Open-loop control of cavity noise using Proper Orthogonal Decomposition reduced-order model

Kaushik Kumar Nagarajan, Sintu Singha, Laurent Cordier, Christophe Airiau

Open-loop control of cavity noise using Proper Orthogonal Decomposition reduced-order model

Kaushik Kumar Nagarajan[a,*], Sintu Singha[a], Laurent Cordier[b], Christophe Airiau[c]

[a] National Aerospace Laboratories, Bengaluru, 560017, India
[b] Institut Pprime, CNRS – Université de Poitiers – ISAE-ENSMA, 86962 Futuroscope Chasseneuil, France
[c] IMFT (Institut de Mécanique des Fluides de Toulouse), UMR 5502 CNRS/INPT-UPS, Université de Toulouse, 2 allée du Pr. Camille Soula, Toulouse, F-31400, France

MSC:
76N25
76M30
76Q05
93A30

Keywords:
Open cavity flow
Optimal control
Noise reduction
Proper Orthogonal Decomposition
Reduced-order modeling

A B S T R A C T

Flow over open cavities is mainly governed by a feedback mechanism due to the interaction of shear layer instabilities and acoustic forcing propagating upstream in the cavity. This phenomenon is known to lead to resonant tones that can reach 180 dB in the far-field and may cause structural fatigue issues and annoying noise emission. This paper concerns the use of optimal control theory for reducing the noise level emitted by the cavity. Boundary control is introduced at the cavity upstream corner as a normal velocity component. Model-based optimal control of cavity noise involves multiple simulations of the compressible Navier–Stokes equations and its adjoint, which makes it a computationally expensive optimization approach. To reduce the computational costs, we propose to use a reduced-order model (ROM) based on Proper Orthogonal Decomposition (POD) as a surrogate model of the forward simulation. For that, a control input separation method is first used to introduce explicitly the control effect in the model. Then, an accurate and robust POD ROM is derived by using an optimization-based identification procedure and generalized POD modes, respectively. Since the POD modes describe only velocities and speed of sound, we minimize a noise-related cost functional characteristic of the total enthalpy unsteadiness. After optimizing the control function with the reduced-order model, we verify the optimality of the solution using the original, high-fidelity model. A maximum noise reduction of 4.7 dB is reached in the cavity and up to 16 dB at the far-field.

1. Introduction

Flow past open cavities is well known to exhibit self-sustained instabilities, leading to an undesirable aeroacoustic noise. These flow-induced oscillations arise from a feedback loop caused by a strong coupling of hydrodynamic instabilities with the acoustic perturbations. In summary, Kelvin-Helmholtz instabilities grow in the separated shear layer, creating coherent structures that impact on the downstream edge of the cavity. This phenomenon radiates acoustic waves that propagate upstream inside the cavity. The high leading edge receptivity causes these unsteady perturbations to further excite the shear layer instabilities. This self-sustained mechanism leads to high noise levels in the far-field and may lead to structural fatigue, optical distortion and annoying noise emission. In engineering applications, cavity flows are encountered in aircraft landing gears, pantograph recess of high speed trains, sunroof of cars, etc. These flows are largely characterized by the presence of a global instability, that dominates the flow, and belong to the oscillators' category as defined by Huerre and Rossi [21]. Reducing the cavity noise is then of extreme importance for the development of quieter transport means. It is now well-known that the control of instabilities for oscillator flows is feasible with a model-based approach relying on linear control tools [35]. In this paper, the objective is to reduce the level of noise emitted by the cavity with an optimal control approach based on a nonlinear model of the dynamics. High-fidelity numerical simulations, like Direct Numerical Simulation (DNS) of Navier–Stokes equations (NSE), are too expensive for flow control applications. This observation is particularly true when iterative optimization methods are used as in the case of optimal control [19]. It is then necessary to derive surrogate models for reducing the computational costs related to optimal control of high-dimensional nonlinear systems. Starting from an experimental or computational database, the objective is to derive Reduced-Order Models (ROMs) which mine the relevant information content in terms of dynamics.

* Corresponding author.
E-mail address: kaushik@ctfd.cmmacs.ernet.in (K.K. Nagarajan).

https://doi.org/10.1016/j.compfluid.2017.10.019

In the last decade, Reduced-Order Models based on Proper Orthogonal Decomposition (POD) have gained a lot of popularity for modeling the dynamics of complex systems [9,10]. These reduced-order models are derived by a Galerkin projection of the governing equations (in our case, the compressible NSE) onto the dominant POD modes. Two main difficulties arise with the use of POD-based ROMs in flow optimization. First, these reduced-order models are in general not sufficiently accurate to describe correctly the original dynamics, even over short periods of time. This is mainly due to the truncation issued from the Galerkin projection where only a small set of POD modes are kept in the model. Second, the POD-based ROMs often exhibit a lack of robustness to the change of control parameters during the optimization procedure. For the accuracy of the model, a variety of numerical strategies have been tested over the years [4,8,11,22,29]. The overall philosophy is to perform a system identification to minimize the error between the solutions obtained by DNS and the one obtained by time integration of the reduced-order model. Concerning the robustness of the model, the ideal would be to derive reduced-order models directly parameterized by the control parameters. However, this is still a matter of development in the reduced-order modeling community [2]. One alternative consists in generating generalized POD functions by forcing the flow with an ad-hoc time dependent excitation that is rich in frequency content. The basic idea is to increase the ability of POD modes to approximate correctly the dynamics corresponding to different actuated flows. This approach was assessed in Bergmann et al. [4] for a circular cylinder wake configuration, where a POD ROM was used to minimize a drag-related cost functional characteristic of the wake unsteadiness. Another alternative is to use an adaptive approach in which new reduced-order models are regularly and automatically determined during the optimization process when the effectiveness of the existing POD-based reduced-order model is insufficient to represent accurately the actuated flow. This approach, called Trust-Region Proper Orthogonal Decomposition (TRPOD), was originally proposed in Fahl [13] and later applied to the drag minimization of a circular cylinder wake flow in Bergmann and Cordier [3]. An interest of TRPOD is the existence of rigorous convergence results which guarantee that the solutions obtained by the TRPOD algorithm converge to the solution of the original optimization problem defined by the high-fidelity model. Regarding the use of Reduced-Order Modeling for flow control, the reader is referred to Noack et al. [27]. An extensive review of closed-loop Turbulence control can be found in the recent paper of Brunton and Noack [6].

Self-sustained oscillations of flow over rectangular cavities have been studied with the aim of understanding the hydrodynamic feedback mechanism that leads to noise emission [5,15,30]. Advances in understanding, modeling, and controlling oscillations in the flow past a cavity have been reviewed in Rowley and Williams [32] with a focus on open- and closed-loop forcing strategies. The model reduction of compressible cavity flows with reduced-order models based on POD has been developed in Rowley et al. [31] and Gloerfelt [14]. In these papers, the main objective is to derive a surrogate model of the compressible Navier–Stokes equations for studying long-time dynamics, or exploring a range of parameters for the unactuated flow. More recently, feedback control of cavity flows using POD-based reduced order models is reported in Samimy et al. [33] and Nagarajan et al. [26]. However, as far as we know, open-loop control of the cavity flow with an optimal control approach based on a reduced-order model derived by POD has not yet been reported in the literature. The target is the reduction of the level of noise emitted by the cavity. A boundary control is introduced at the cavity upstream corner as a normal velocity component to simulate a zero mass flow synthetic jet type actuation. Since the POD modes represent only the velocity components and the speed of sound, a noise-related cost functional characteristic of the total enthalpy unsteadiness is minimized. The accuracy and the robustness of the POD-based reduced-order model are improved by an identification procedure and the use of generalized POD modes, respectively. The optimal control approach is solved using a classical Lagrange multipliers method. The performance of the optimized solution is evaluated by introducing the control law into the DNS simulation. The efficiency of the open-loop control is measured by introducing pressure sensors at various locations of the cavity in the near and far field, and by computing the spectra of pressure signals. Finally, the far-field acoustics is characterized by estimating the Overall Sound Pressure Level (OASPL).

This article is organized as follows: in Section 2, a framework for applying POD and Galerkin projection to compressible fluids is presented. The extension of this formalism to the case of actuated flows, and the identification technique used for improving the accuracy of the model are also briefly discussed. The optimal control approach used in this paper for determining the open-loop control law is described in Section 3. In Section 4, the applications of reduced-order modeling for the unactuated and optimized actuated flows are presented. Some concluding remarks and perspectives follow in Section 5.

2. Reduced-order modeling based on Proper Orthogonal Decomposition

The principle of Proper Orthogonal Decomposition is to extract modes based on optimizing the mean square of the field variable being examined [9]. POD is one of the most widely used techniques in analyzing fluid flows. Beyond this, an attractive property of POD is its potential for constructing reduced-order models [10]. Indeed, Galerkin projection can be used to reduce high-dimensional discretization of partial differential equations into reduced-order models made of ordinary differential equations. Let Ω be the spatial domain and $\boldsymbol{q}(\boldsymbol{x}, t)$ any vector field of interest (e.g., velocity) where $\boldsymbol{x}$ and t represent space and time, respectively. We seek a space-time decomposition of $\boldsymbol{q}$ in the form:

$$\boldsymbol{q}(\boldsymbol{x}, t) = \bar{\boldsymbol{q}}(\boldsymbol{x}) + \sum_{i=1}^{N_{\text{Snap}}} a_i^P(t)\boldsymbol{\phi_i}(\boldsymbol{x}), \tag{1}$$

where $\bar{\boldsymbol{q}}$ represents the ensemble average of a set of N_{Snap} flow snapshots. The spatial modes $\boldsymbol{\phi_i}$ and the temporal coefficients a_i^P are determined as the solutions of a constrained optimization problem [7]. It can be shown that these modes can be determined by a singular value decomposition of the data matrix that collects an ensemble of snapshots at different time instants [20]. The POD modes can then be exploited in a Galerkin framework to derive a reduced-order model by projection of the governing equations onto the dominant modes. The flow past a cavity is here modeled with the same compressible isentropic equations as in Rowley et al. [31]. According to the usual compressible non-dimensionalization, the length scales are non-dimensionalized with the cavity depth D, the streamwise and spanwise velocity components, u and v, with the free stream velocity U_∞, and the speed of sound c by the free stream sound speed c_∞. The isentropic Navier–Stokes equations may be written in two dimensions as

$$\begin{aligned}
u_t &= -uu_x - vu_y - \frac{1}{\mathrm{M}^2}\frac{2}{\gamma-1}cc_x + \frac{1}{\mathrm{Re}}(u_{xx}+u_{yy}) \\
v_t &= -uv_x - vv_y - \frac{1}{\mathrm{M}^2}\frac{2}{\gamma-1}cc_y + \frac{1}{\mathrm{Re}}(v_{xx}+v_{yy}) \\
c_t &= -uc_x - vc_y - \frac{\gamma-1}{2}c(u_x+v_y),
\end{aligned}$$

where $\mathrm{Re} = U_\infty D/\nu$ is the Reynolds number and $\mathrm{M} = U_\infty/c_\infty$ is the Mach number. In these equations, the indices t, x and y stand for partial derivation.

Denoting $\boldsymbol{q} = (u, v, c)$, these equations take the form:

$$\dot{\boldsymbol{q}} = \frac{1}{\mathrm{Re}}\boldsymbol{L}(\boldsymbol{q}) + \frac{1}{\mathrm{M}^2}\boldsymbol{Q_1}(\boldsymbol{q},\boldsymbol{q}) + \boldsymbol{Q_2}(\boldsymbol{q},\boldsymbol{q}) \qquad \text{with} \tag{2}$$

$$\boldsymbol{L}(\boldsymbol{q}) = \begin{bmatrix} u_{xx}+u_{yy} \\ v_{xx}+v_{yy} \\ 0 \end{bmatrix}, \boldsymbol{Q_1}(\boldsymbol{q^1},\boldsymbol{q^2}) = -\frac{2}{\gamma-1}\begin{bmatrix} c^1c^2_x \\ c^1c^2_y \\ 0 \end{bmatrix},$$

$$\text{and} \quad \boldsymbol{Q_2}(\boldsymbol{q^1},\boldsymbol{q^2}) = -\begin{bmatrix} u^1u^2_x + v^1u^2_y \\ u^1v^2_x + v^1v^2_y \\ u^1c^2_x + v^1c^2_y + \dfrac{\gamma-1}{2}c^1(u^2_x+v^2_y) \end{bmatrix}.$$

In order to obtain vector-valued POD modes, and then derive a reduced-order model by Galerkin projection, we must first define an inner product. An appropriate choice for compressible flows is to consider:

$$\left(\boldsymbol{q^1},\boldsymbol{q^2}\right)_\Omega = \int_\Omega (u^1u^2 + v^1v^2 + \frac{2}{\gamma-1}c^1c^2)\,\mathrm{d}\boldsymbol{x}, \tag{3}$$

where γ is the ratio of specific heats. This definition gives stagnation enthalpy as the induced norm. Another advantage of using (3) for definition is that the origin of the attractor of the reduced-order model remains stable as shown in Rowley et al. [31]. Inserting the expansion (1) into (2), and taking the inner product with $\boldsymbol{\phi_i}$ gives

$$\begin{aligned}
\dot{a}^R_i(t) &= \underbrace{\frac{1}{\mathrm{Re}}C^1_i + \frac{1}{\mathrm{M}^2}C^2_i + C^3_i}_{C_i} + \sum_{j=1}^{N_{\mathrm{Gal}}} \underbrace{\left(\frac{1}{\mathrm{Re}}L^1_{ij} + \frac{1}{\mathrm{M}^2}L^2_{ij} + L^3_{ij}\right)}_{L_{ij}} a^R_j(t) \\
&\quad + \sum_{j,k=1}^{N_{\mathrm{Gal}}} \underbrace{\left(\frac{1}{\mathrm{M}^2}Q^1_{ijk} + Q^2_{ijk}\right)}_{Q_{ijk}} a^R_j(t)a^R_k(t) \\
&= C_i + \sum_{j=1}^{N_{\mathrm{Gal}}} L_{ij}a^R_j(t) + \sum_{j,k=1}^{N_{\mathrm{Gal}}} Q_{ijk}a^R_j(t)a^R_k(t) \\
&= f_i(\underbrace{C_i, \boldsymbol{L_i}, \boldsymbol{Q_i}}_{\boldsymbol{y}_i}, \boldsymbol{a}^R(t)) = f_i(\boldsymbol{y}_i, \boldsymbol{a}^R(t))
\end{aligned} \tag{4}$$

where f_i is a polynomial of degree 2 in $\boldsymbol{a}^R$, and where N_{Gal} is the number of POD modes kept in the projection. The coefficients of the dynamical system are given by

$$\begin{aligned}
C^1_i &= \left(\boldsymbol{\phi_i}, \boldsymbol{L}(\overline{\boldsymbol{q}})\right)_\Omega, & L^1_{ij} &= \left(\boldsymbol{\phi_i}, \boldsymbol{L}(\boldsymbol{\phi_j})\right)_\Omega, \\
C^2_i &= \left(\boldsymbol{\phi_i}, \boldsymbol{Q_1}(\overline{\boldsymbol{q}},\overline{\boldsymbol{q}})\right)_\Omega, & L^2_{ij} &= \left(\boldsymbol{\phi_i}, \boldsymbol{Q_1}(\overline{\boldsymbol{q}},\boldsymbol{\phi_j}) + \boldsymbol{Q_1}(\boldsymbol{\phi_j},\overline{\boldsymbol{q}})\right)_\Omega, \\
C^3_i &= \left(\boldsymbol{\phi_i}, \boldsymbol{Q_2}(\overline{\boldsymbol{q}},\overline{\boldsymbol{q}})\right)_\Omega, & L^3_{ij} &= \left(\boldsymbol{\phi_i}, \boldsymbol{Q_2}(\overline{\boldsymbol{q}},\boldsymbol{\phi_j}) + \boldsymbol{Q_2}(\boldsymbol{\phi_j},\overline{\boldsymbol{q}})\right)_\Omega, \quad \text{and}
\end{aligned}$$

$$\begin{aligned}
Q^1_{ijk} &= \left(\boldsymbol{\phi_i}, \boldsymbol{Q_1}(\boldsymbol{\phi_j},\boldsymbol{\phi_k})\right)_\Omega, \\
Q^2_{ijk} &= \left(\boldsymbol{\phi_i}, \boldsymbol{Q_2}(\boldsymbol{\phi_j},\boldsymbol{\phi_k})\right)_\Omega.
\end{aligned}$$

The temporal dynamics of the coefficients a^R_i can now be determined by a time integration of (4) from the initial conditions $a^P_i(0)$ directly obtained by POD. For that, a fourth order Runge–Kutta scheme is used.

Since the main goal of deriving a POD-based reduced-order model is flow control, we need to extend the previous formalism by explicitly introducing the control in the model. Following Kasnakoglu [23], we seek [26] an orthogonal basis expansion given by

$$\boldsymbol{q}(\boldsymbol{x},t) = \overline{\boldsymbol{q}}(\boldsymbol{x}) + \tilde{\boldsymbol{q}}^{\mathrm{ac}}(\boldsymbol{x},t) + \gamma(t)\boldsymbol{\psi}(\boldsymbol{x}), \tag{5}$$

with

$$\tilde{\boldsymbol{q}}^{\mathrm{ac}}(\boldsymbol{x},t) = \sum_{i=1}^{N_{\mathrm{Gal}}} a^{\mathrm{ac}}_i(t)\boldsymbol{\phi_i}(\boldsymbol{x}), \tag{6}$$

and where γ and $\boldsymbol{\psi}$ represent the actuation and the actuated spatial mode, respectively. In (5), $\overline{\boldsymbol{q}}$ is the mean field defined in (1), and $\boldsymbol{\phi_j}$ are the spatial eigenfunctions of the uncontrolled flow. $\boldsymbol{\psi}$ is determined as a solution of an unconstrained minimization problem as detailed in Kasnakoglu [23] and Nagarajan et al. [26]. Substituting (5) into (2) and then carrying out Galerkin projection yields the following reduced-order model for the actuated dynamics:

$$\begin{aligned}
\dot{a}^{\mathrm{ac}}_i(t) &= C_i + \sum_{j=1}^{N_{\mathrm{Gal}}} L_{ij}a^{\mathrm{ac}}_j(t) + \sum_{j,k=1}^{N_{\mathrm{Gal}}} Q_{ijk}a^{\mathrm{ac}}_j(t)a^{\mathrm{ac}}_k(t) \\
&\quad + h_{1i}\gamma(t) + \sum_{j=1}^{N_{\mathrm{Gal}}} h_{2ij}a^{\mathrm{ac}}_j(t)\gamma(t) + h_{3i}\gamma^2(t).
\end{aligned} \tag{7}$$

The coefficients of this model are given by

$$\begin{aligned}
h_{1i} &= \frac{1}{\mathrm{Re}}\left(\boldsymbol{\phi_i}, \boldsymbol{L}(\boldsymbol{\psi})\right)_\Omega + \left(\boldsymbol{\phi_i}, \boldsymbol{Q}(\overline{\boldsymbol{q}},\boldsymbol{\psi})\right)_\Omega + \left(\boldsymbol{\phi_i}, \boldsymbol{Q}(\boldsymbol{\psi},\overline{\boldsymbol{q}})\right)_\Omega, \\
h_{2ij} &= \left(\boldsymbol{\phi_i}, \boldsymbol{Q}(\boldsymbol{\phi_j},\boldsymbol{\psi})\right)_\Omega + \left(\boldsymbol{\phi_i}, \boldsymbol{Q}(\boldsymbol{\psi},\boldsymbol{\phi_j})\right)_\Omega, \\
h_{3i} &= \left(\boldsymbol{\phi_i}, \boldsymbol{Q}(\boldsymbol{\psi},\boldsymbol{\psi})\right)_\Omega,
\end{aligned}$$

with $\boldsymbol{Q}(\cdot,\cdot) = \frac{1}{\mathrm{M}^2}\boldsymbol{Q_1}(\cdot,\cdot) + \boldsymbol{Q_2}(\cdot,\cdot)$. It is well-known that a POD-based reduced-order modeling is in general not sufficiently accurate to describe the correct dynamics of the original flow. This is true for uncontrolled flows where convergence to wrong attractors, and even divergence, have been reported for long time integration [36]. This phenomenon is even more likely to occur when the goal of POD reduced-order models is to reproduce actuated flows. This inaccuracy is mainly attributed to the mode truncation effect introduced by the Galerkin projection. Many strategies have been considered in the literature to treat these shortcomings. Among them, different identification methods have been proposed in Cordier et al. [8]. The principle of these methods is to determine the coefficients $\boldsymbol{y}_i$ $(i = 1, \cdots, N_{\mathrm{Gal}})$ in (4) such that the error between the temporal POD coefficients $a^P_i(t)$ determined by POD, and those obtained by time integration of (4) is minimized in a given sense. In this work, a weighted regularization approach as in Nagarajan et al. [26] is used to calibrate the coefficients of the reduced-order model.

3. Open-loop control of cavity flows

In this section, an optimal control approach is used to determine the control γ. A cost functional $\mathcal{C}$, which includes the control objective as well as the cost of introducing the control, is minimized over an optimization time horizon T_o. A detailed description of optimal control theory can be found in Gunzburger [17], [18] and Cordier [7]. The main obstacle to the use of optimal control is the high computational costs associated with the solution when a high-fidelity model is used to describe the dynamics of the system. For that reason, the POD reduced-order model (7) is here employed as a low-dimensional approximation model of the actuated dynamics. Since only the velocity components and the speed of sound are represented by the POD modes, it seems natural to use the total stagnation enthalpy of the fluctuating state variable $\tilde{\boldsymbol{q}}^{\mathrm{ac}}$ as a proxy for the cavity noise. Mathematically, this goal is represented by the cost function:

$$\mathcal{C}(\boldsymbol{q},\gamma) = \frac{\ell_1}{2}\int_0^{T_o} \|\tilde{\boldsymbol{q}}^{\mathrm{ac}}(\boldsymbol{x},t)\|^2_\Omega\,\mathrm{d}t + \frac{\ell_2}{2}\int_0^{T_o}\gamma^2(t)\,\mathrm{d}t. \tag{8}$$

The first term on the right hand side corresponds to the control goal and the second term represents the cost associated with the control. The real constants ℓ_1 and ℓ_2 are the regularization parameters which are arbitrarily chosen to limit the size of control and

to define a well-posed optimization problem. Substituting $\tilde{\boldsymbol{q}}^{\mathrm{ac}}$ with the POD expansion (6) yields to:

$$\begin{aligned}\mathcal{C}(\boldsymbol{a}^{\mathrm{ac}},\gamma) &= \frac{\ell_1}{2}\int_0^{T_o}\|\boldsymbol{a}^{\mathrm{ac}}(t)\|_2^2\,\mathrm{d}t + \frac{\ell_2}{2}\int_0^{T_o}\gamma^2(t)\,\mathrm{d}t \\ &= \frac{\ell_1}{2}\int_0^{T_o}\sum_{i=1}^{N_{\mathrm{Gal}}}\left(a_i^{\mathrm{ac}}\right)^2(t)\,\mathrm{d}t + \frac{\ell_2}{2}\int_0^{T_o}\gamma^2(t)\,\mathrm{d}t. \end{aligned} \tag{9}$$

The original control problem is then expressed as

$$\begin{cases}\min\limits_{\gamma(t)} \mathcal{C}(\boldsymbol{a}^{\mathrm{ac}},\gamma(t)) \\ \quad \text{constrained to} \\ \boldsymbol{\mathcal{S}}(\boldsymbol{a}^{\mathrm{ac}},\gamma(t)) = \boldsymbol{0},\end{cases} \tag{10}$$

where the constraint $\boldsymbol{\mathcal{S}}$ is given by the actuated reduced-order model (7). The Lagrange multipliers method is used to solve this constrained optimization problem. For enforcing the constraints, Lagrange multipliers also referred to as the adjoint variables $\boldsymbol{\xi}$ are introduced, and a new Lagrangian functional is defined as

$$\begin{aligned}\mathcal{A}(\boldsymbol{a}^{\mathrm{ac}},\gamma,\boldsymbol{\xi}) &= \mathcal{C}(\boldsymbol{a}^{\mathrm{ac}},\gamma(t)) - \langle\boldsymbol{\xi},\boldsymbol{\mathcal{S}}(\boldsymbol{a}^{\mathrm{ac}},\gamma)\rangle \\ &= \mathcal{C}(\boldsymbol{a}^{\mathrm{ac}},\gamma(t)) - \sum_{i=1}^{N_{\mathrm{Gal}}}\int_0^{T_o}\xi_i(t)\mathcal{S}_i(\boldsymbol{a}^{\mathrm{ac}},\gamma)\,\mathrm{d}t. \end{aligned} \tag{11}$$

The main purpose of introducing the Lagrangian functional $\mathcal{A}$ is to transform the constrained optimization problem (10) into an unconstrained optimization problem that is easier to solve. The solutions of this new optimization problem are obtained at the stationary points of $\mathcal{A}$ *i.e.* for

$$\delta\mathcal{A} = \sum_{i=1}^{N_{\mathrm{Gal}}}\left(\frac{\partial\mathcal{A}}{\partial a_i^{\mathrm{ac}}}\delta a_i^{\mathrm{ac}}\right) + \frac{\partial\mathcal{A}}{\partial\gamma}\delta\gamma + \sum_{i=1}^{N_{\mathrm{Gal}}}\left(\frac{\partial\mathcal{A}}{\partial\xi_i}\delta\xi_i\right) = 0$$

where $\delta\boldsymbol{a}^{\mathrm{ac}}$, $\delta\gamma$ and $\delta\boldsymbol{\xi}$ are arbitrary variations for the state, control and the adjoint variables, respectively.

The so-called optimality system is finally obtained by setting each variation of $\mathcal{A}$ with respect to the parameters $\boldsymbol{\xi}$, $\boldsymbol{a}^{\mathrm{ac}}$ and γ to zero. Collecting the results, we obtain:

$$\boldsymbol{\mathcal{S}}(\boldsymbol{a}^{\mathrm{ac}},\gamma(t)) = \boldsymbol{0}, \tag{12a}$$

$$\begin{aligned}\frac{d\xi_i(t)}{dt} &= -\ell_1 a_i^{\mathrm{ac}}(t) \\ &\quad -\sum_{j=1}^{N_{\mathrm{Gal}}}\left(L_{ji}+\gamma(t)h_{2ji}+\sum_{k=1}^{N_{\mathrm{Gal}}}\left(Q_{jik}+Q_{jki}\right)a_k^{\mathrm{ac}}(t)\right)\xi_j(t)\end{aligned} \tag{12b}$$

$$\frac{\partial\mathcal{A}}{\partial\gamma} = \ell_2\gamma(t) + \sum_{i=1}^{N_{\mathrm{Gal}}}\left(h_{1i}+\sum_{j=1}^{N_{\mathrm{Gal}}}h_{2ij}a_j^{\mathrm{ac}} + 2h_{3i}\gamma(t)\right)\xi_i. \tag{12c}$$

These equations, namely the state Eq. (12a), the adjoint Eq. (12b) and the optimality condition (12c), are collectively referred to as the optimality system. At the minimum of $\mathcal{C}$, the optimality condition is equal to zero. The adjoint equation is solved backward in time from the terminal condition

$$\xi_i(T_o) = 0.$$

The optimality system (12) is solved iteratively. The algorithm is the following: start with an initial guess $\gamma^{(0)}(t)$ for the control parameter. For $m = 0, 1, 2, \ldots, +\infty$

1. Solve the direct system (12a) forward in time to obtain the corresponding state variables $(\boldsymbol{a}^{\mathrm{ac}})^{(m)}(t)$.
2. Use the direct variables obtained in step 1 to solve the adjoint system (12b) for $\boldsymbol{\xi}^{(m)}(t)$.
3. Use the results of step 1 and 2 to compute the gradient of the functional $\nabla_\gamma\mathcal{C}^{(m)}(t)$ on the interval $[0;\, T_o]$ by solving the optimality condition (12c).

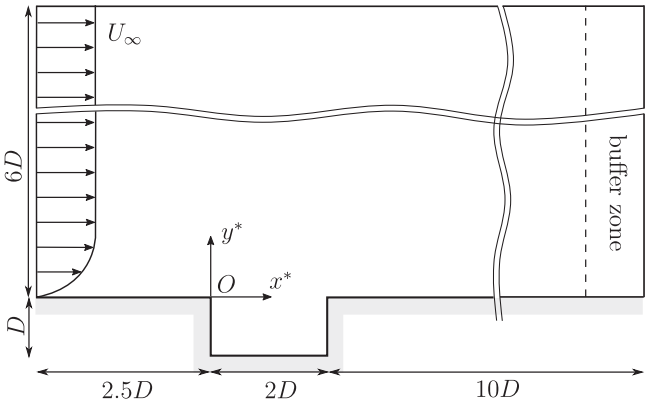

Fig. 1. Geometry and computational domain with dimensional quantities.

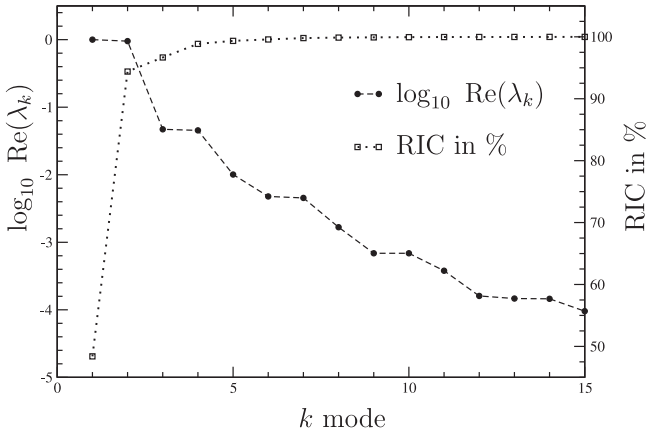

Fig. 2. POD eigenvalues and Relative Information Content (RIC). Only the first 15 modes are shown.

4. Use the gradient determined in the previous step to update the control. Set $\gamma^{(m+1)}(t) = \gamma^{(m)}(t) + \omega^{(m)}\boldsymbol{d}^{(m)}(t)$ where $\boldsymbol{d}^{(m)}$ is a direction of descent estimated by a conjugate gradient method, using $\nabla_\gamma\mathcal{C}^{(m)}(t)$. Here $\omega^{(m)}$ is the length step determined by the Armijo method.
5. Repeat the procedure until a suitable stopping criterion is satisfied.

4. Results and discussions

4.1. Reduced-order modeling of the unactuated flow

The two-dimensional, compressible flow past a rectangular cavity is considered. Fig. 1 describes the computational domain. The flow conditions are for a Mach number M = 0.6, length to depth ratio equal 2, a Reynolds number based on the cavity depth of Re = 1500 [26]. A zero-pressure gradient laminar boundary layer is defined at the domain inlet to ensure a thickness of $\delta = 0.28D$ on the left cavity corner. A 4th order predictor corrector scheme for both the temporal and spatial discretization as given in Gottlieb and Turkel [16] is used. No-slip boundary conditions are applied along the walls. In addition, the characteristic boundary conditions are implemented to avoid acoustic wave reflections on open boundaries of the computational domain and a buffer region is added at the outlet of the domain to damp any residual numerical waves [25]. After verification of mesh convergence, 48,180 cells have been chosen for the computation.

A total of $N_{\mathrm{Snap}} = 56$ snapshots uniformly sampled over one period of the oscillation (around 2.8 non dimensional time) are taken after the decay of transient flow. Fig. 2 shows the POD eigenvalue

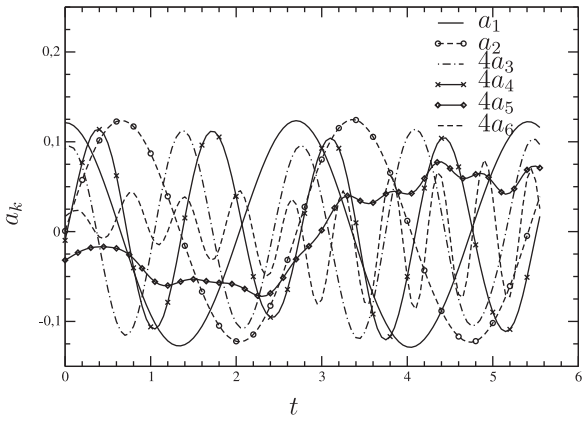

Fig. 3. Time evolution of the first 6 POD coefficients. Modes a_3 to a_6 are scaled up by a factor of 4.

spectrum and the Relative Information Content (RIC) defined as $\mathrm{RIC}(i) = \sum_{j=1}^{i} \lambda_j / \sum_{j=1}^{N_{\mathrm{Snap}}} \lambda_j$ where λ_j is the jth POD eigenvalue. The convergence of the POD eigenspectrum is fast: 6 modes are sufficient to represent 98.5% of the total fluctuation enthalpy. Clearly, the first four eigenvalues occur in pairs of almost equal values, a characteristic of convection-dominated flows. Modes 5, 8 and 11 are isolated in the spectrum and split up groups of two modes of almost equal energy. Finally, starting from mode 12, modes are merged into triplets of same energy. The contribution of all these higher modes is very low not only in terms of energy but also the dynamics. In Fig. 3, we present the time evolution of the first six temporal coefficients a_k. As expected, the phase difference of the temporal modes corresponding to the paired eigenvalues is around $\pi/2$. Moreover, in agreement with the POD eigenspectrum, the fast damping of the higher time coefficients can be observed. Mode 5 exhibits a different dynamic behavior, in a similar way to modes 8 and 11 (not shown here). This point remains largely unexplained and deserves further numerical studies. A possible explanation may be a numerical adjustment of the higher POD modes to better capture the low amplitude and low frequency flow dynamics not described by the most energetic modes.

The vorticity contours of the first three pairs of spatial POD modes are represented in Fig. 4. As expected, a phase shift between odd and even modes can be observed in the cavity, in the shear layer and downstream of the wall boundary layer. The spatial organization of mode 5 seems similar to the other modes, suggesting that this mode provides only a time amplitude adjustment with respect to the reference high-fidelity flow data. We see that the vorticity is mainly concentrated in the shear layer, the boundary layer and the separated flow regions inside the cavity. On the downstream cavity corner, the impact of the shear layer strongly modifies the vorticity distribution along both the vertical and downstream horizontal wall boundary layers. Since the vorticity flux at a wall is strongly related to the tangential pressure gradient, the local unsteadiness of the wall vorticity flux can be associated to strong pressure fluctuations and therefore can be considered as the origin of the noise emission at the corner. This corresponds to the low frequency dynamics of the flow. The thin layer of alternative positive and negative vorticity, visible just after the downstream corner ($2 \leq x \leq 4$), indicates the presence of a separation. A topological equivalence of the modes correspond-

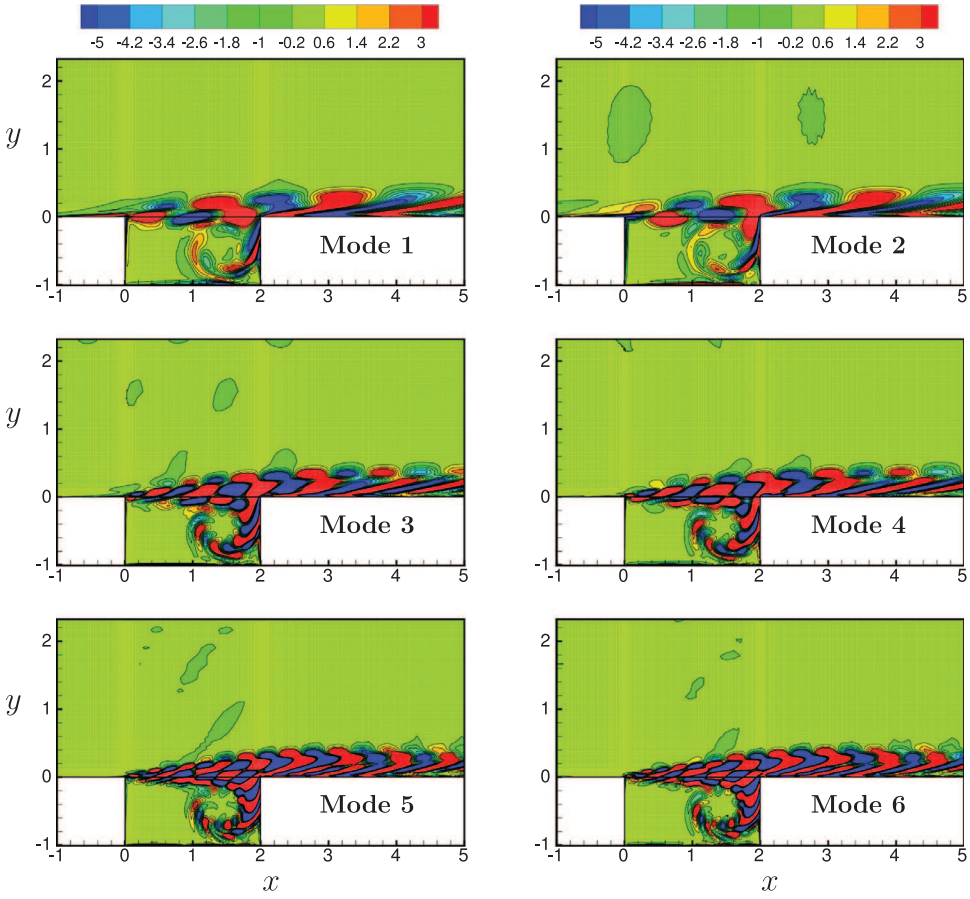

Fig. 4. Vorticity contours of the first three pairs of POD modes.

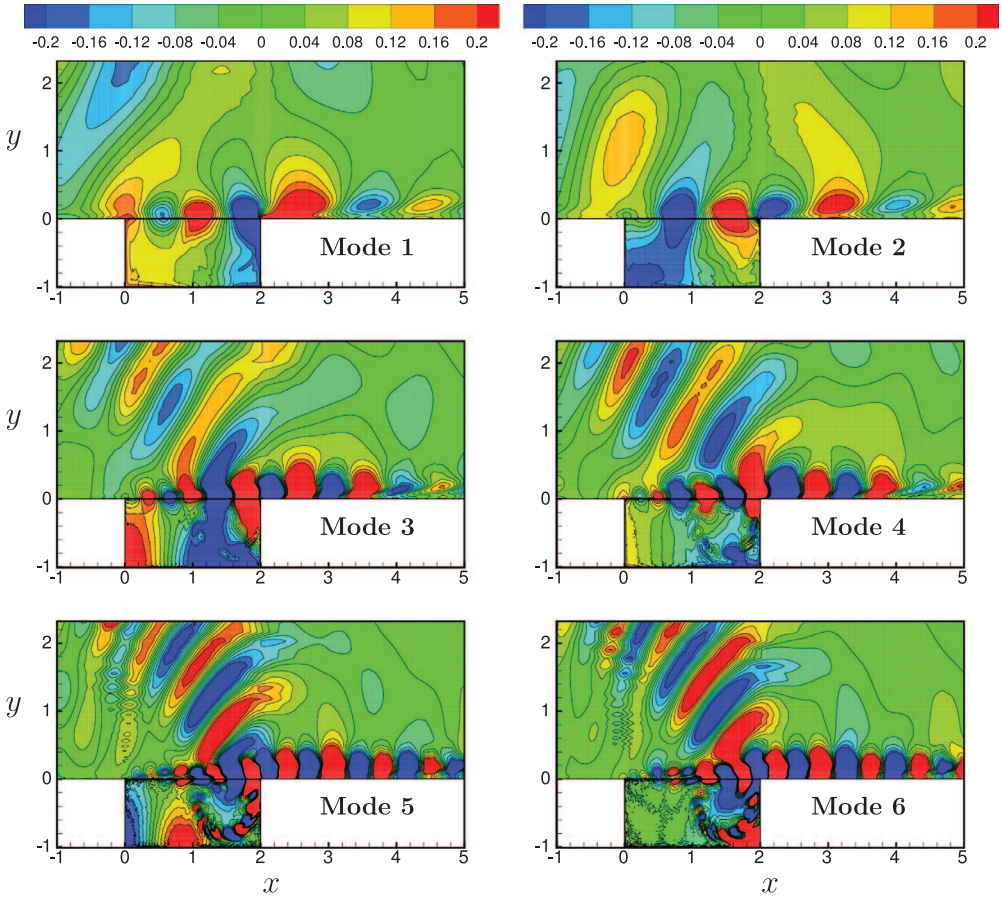

Fig. 5. Dilatation contours for the first three pairs of POD modes.

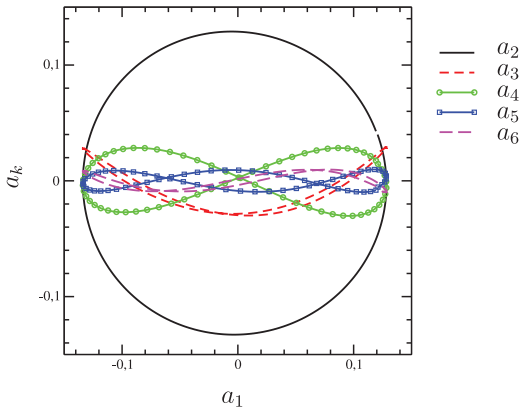

Fig. 6. Phase portraits of the first POD modes for $k = 2$–6.

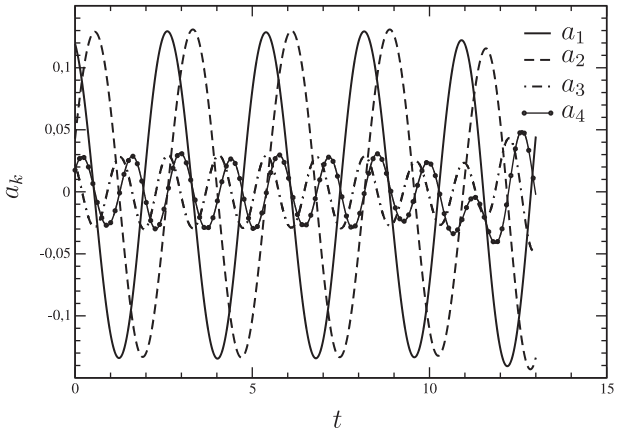

Fig. 7. Time evolution of the first four temporal POD coefficients over a time window greater than the one corresponding to the validity of the POD ROM. The reduced-order model diverges at $t \approx 11$.

ing to the paired eigenvalues is also observed. To spatially represent the high frequency range, we introduce the volumetric dilatation rate defined in 2D as $\nabla \cdot \boldsymbol{u}$. The dilatation reveals the directivity of sound propagation radiated from the downstream corner, as shown in Fig. 5 for the first six POD modes. A wave propagation directivity of 135° is observed as reported in Rowley et al. [30]. An increase of frequency content with the POD mode number is clearly visible. It is also worthwhile to note that the single-frequency Kelvin-Helmholtz shear layer instabilities do not seem to contribute mainly to the noise emission.

Fig. 6 represents the phase portraits of the reduced-order model (4) after identification of the coefficients with the calibration procedure described in Nagarajan et al. [26]. A very good agreement between the temporal coefficients coming from the identified model and the ones directly determined by POD has been obtained for a time horizon corresponding to the snapshots acquisition period (not shown here). All the curves are closed, shedding light on the oscillatory characteristic of the flow. The identified ROM model is expected to be valid over a much longer time horizon. However, as reported in Sirisup and Karniadakis [36], even with a correct state initialization of the reduced-order model, the solution may drift away after many time periods. Fig. 7 illustrates that

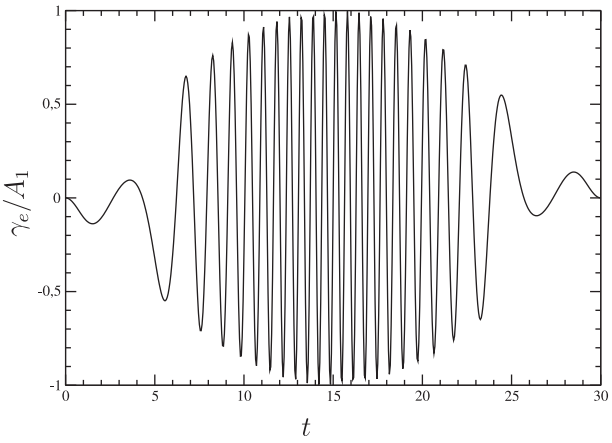

Fig. 8. Temporal excitation γ_e imposed to the cavity simulation for extracting the POD modes used in the resolution of the optimal control problem.

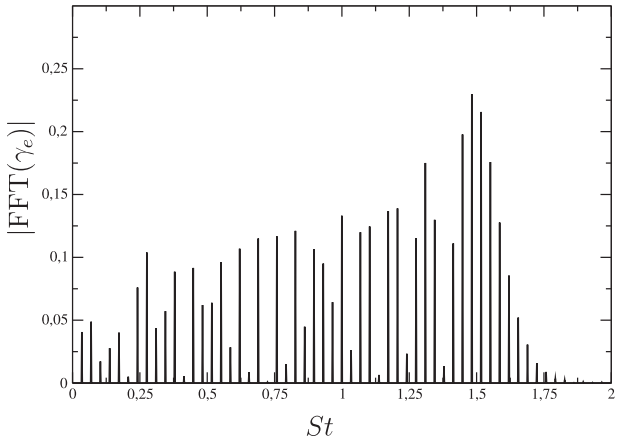

Fig. 9. Amplitude of the Fast Fourier Transform (FFT) of the temporal excitation γ_e.

the identified model correctly represents the dynamics until $t \simeq 11$ after which there is a rapid divergence. It is noticeable that the divergence begins with the higher POD mode. Since the time horizon of the optimal control process is usually much larger than the flow period, the reduced-order model has been identified for a much larger time horizon, see Nagarajan et al. [26].

4.2. Reduced-order modeling for the actuated flow

The main difficulty of using a reduced-order model based on POD as approximate model to solve an optimization problem is the lack of robustness of the model when it is used for values of the control parameters different than the ones employed for deriving it. Two strategies are then possible. First, the reduced-order model can be derived once for all and used throughout the optimization process. In that case, it is necessary to give special attention to the derivation of the model, and more especially to the snapshots that are used for determining the POD modes, see Bergmann et al. [4] for instance. The second strategy is to update the reduced-order models during the optimization process. For that, the trust-region proper orthogonal decomposition (TRPOD) approach can be implemented as it was done in Bergmann and Cordier [3]. In this paper, we decide to follow the procedure proposed in Bergmann et al. [4] and to derive generalized POD modes that correspond to an *ad hoc* forcing term rich in frequency content. A good choice is the so-called "chirp" function. Mathematically, it can be represented by the temporal excitation γ_e defined as:

$$\gamma_e(t) = A_1 \sin(2\pi St_1 t) \times \sin\left(2\pi St_3 t - A_2 \sin(2\pi St_2 t)\right), \qquad (13)$$

where $A_1 = 0.1$, $A_2 = 27$, $St_1 = 1/60$, $St_2 = 1/30$ and $St_3 = 2/3$ (see Fig. 8). A new DNS simulation is then performed with the forcing γ_e introduced at the cavity upstream corner ($x/D \in \Omega_c = [-0.15; -0.05]$) where the flow is most sensitive to external disturbances [24]. The actuation is modeled as a normal velocity component $v_w(\boldsymbol{x}, t) = \gamma_e(t) s(\boldsymbol{x})$ where s is equal to a sine function for $\boldsymbol{x} \in \Omega_c$ and zero elsewhere. The choice of a sine function for s ensures the continuity of derivative for the wall normal velocity. The spectrum of the chirp function γ_e is shown in Fig. 9. The frequency content is determined as the amplitude of the Fast Fourier Transform of the RMS signal. To improve the spectral resolution, the signal is periodized over a time window equal to 20 time periods of γ_e. The frequencies vary in the range $0.5 - 1.6$ with a dominant frequency[1] at 1.5.

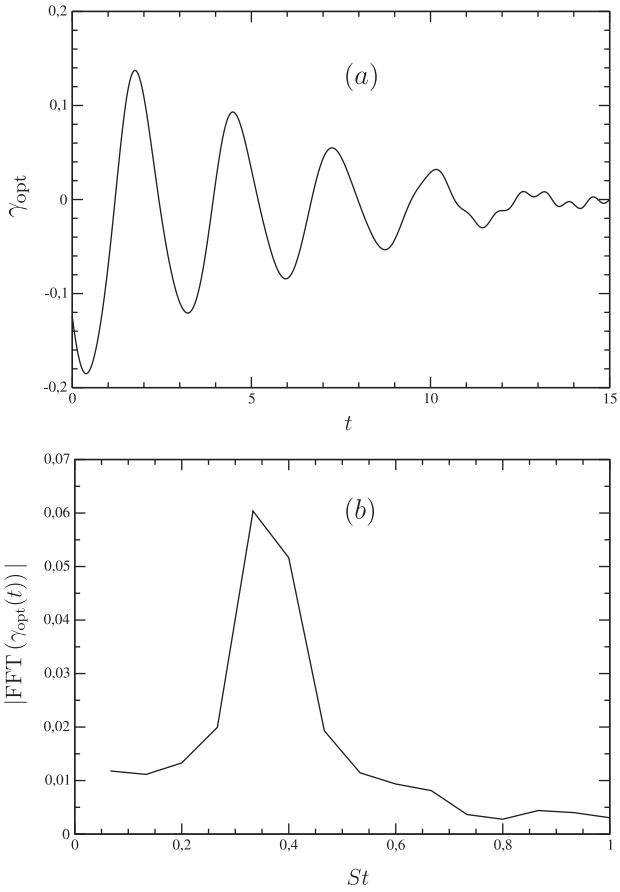

Fig. 10. Optimized control function γ_{opt}: (a) time evolution signal and (b) amplitude of the corresponding FFT.

To compute the actuated spatial mode $\boldsymbol{\psi}$, 600 snapshots are collected evenly from the DNS over a non-dimensional time $T_e = 30$ that corresponds to one period of the chirp excitation. The optimal control approach described in Section 3 is then solved for $\ell_1 = 1$ and $\ell_2 = 0$. This choice corresponds to the case where the cost of the actuators is neglected. This simplification is justified

[1] In our simulations, the length scales are non-dimensionalized by the cavity depth ($D = 1$) and the velocities by $U_\infty = 1$. Therefore the term frequency and Strouhal number is used interchangeably.

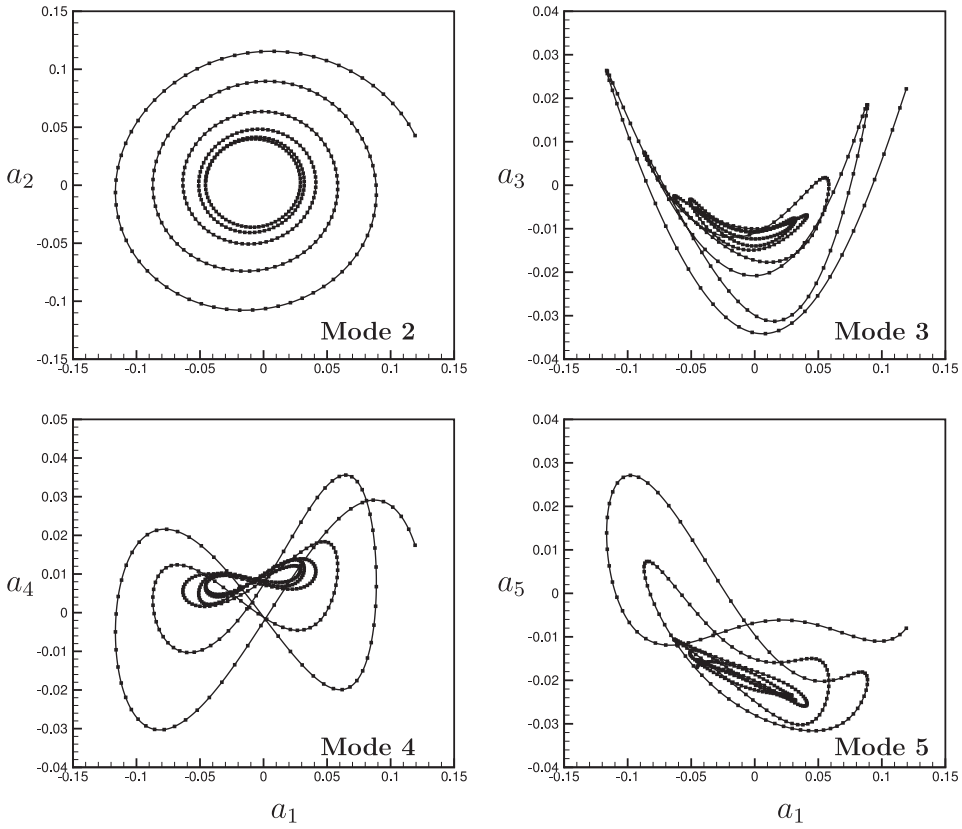

Fig. 11. Phase portraits of the optimized controlled flow for modes 2–5 with respect to mode 1.

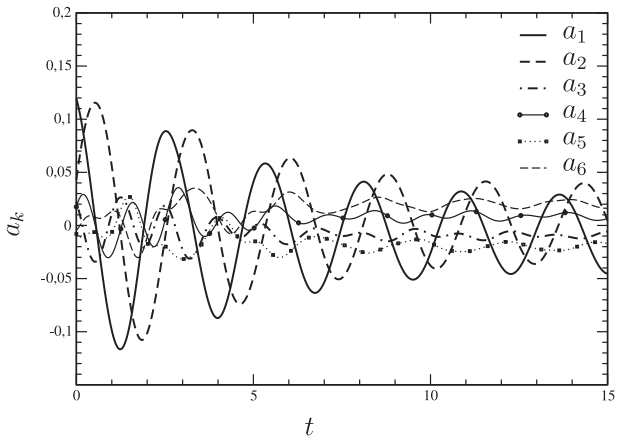

Fig. 12. Time evolution of the first six temporal POD coefficients obtained for the optimized control law $\gamma_{\text{opt}}(t)$.

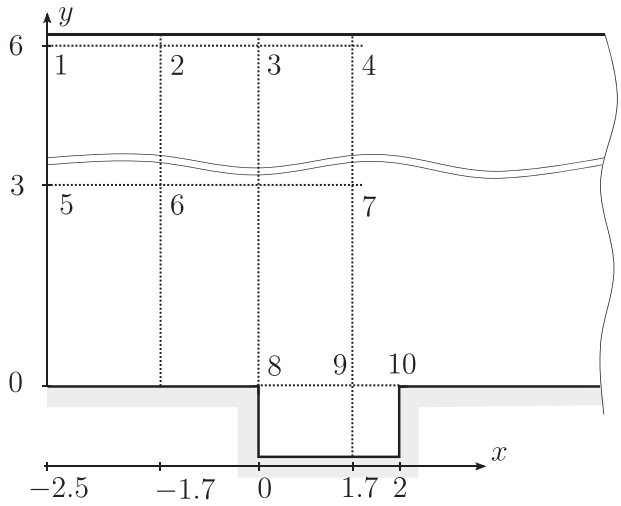

Fig. 13. Locations of the pressure sensors inside the cavity in non-dimensional coordinates.

since we are not interested in the energetic efficiency but rather to attain the smallest possible value of the objective functional. The iterative algorithm described at the end of Section 3 is applied with $T_o = 15$. The procedure stops when the change in the value of $\mathcal{C}$ is less than 10^{-5} between two successive iterations, *i.e.* when $|\Delta\mathcal{C}(\boldsymbol{a}^{\text{act}}, \gamma)| = |\mathcal{C}^{(m+1)}(\boldsymbol{a}^{\text{act}}, \gamma) - \mathcal{C}^{(m)}(\boldsymbol{a}^{\text{act}}, \gamma)| \leq 10^{-5}$. The convergence is obtained after 900 iterations corresponding to a CPU time of around 1000 s. For the whole optimization procedure, including the generation of snapshots, the computational time is around 14 h on an Intel Xeon 5670 processor. The vast majority of this time is employed by the DNS simulation for producing the actuated snapshots. Performing an optimal control approach with the full Navier–Stokes equations and their adjoint would require few days, since the computational cost of solving the adjoint NSE is approximately the same as solving the NSE [24]. In addition, it should be noticed that the direct state should be saved on the whole grid at every time step to solve the adjoint NSE. In conclusion, a huge saving in computational time and memory is made with the POD ROM based optimization.

The time evolution of the optimized control function γ_{opt} and its associated spectrum are plotted in Fig. 10(a) and (b), respectively. The actuation tends to zero at the end of the optimization time window. This is a sign that a new converged state is obtained in the phase space (see the discussion later). The optimal solution

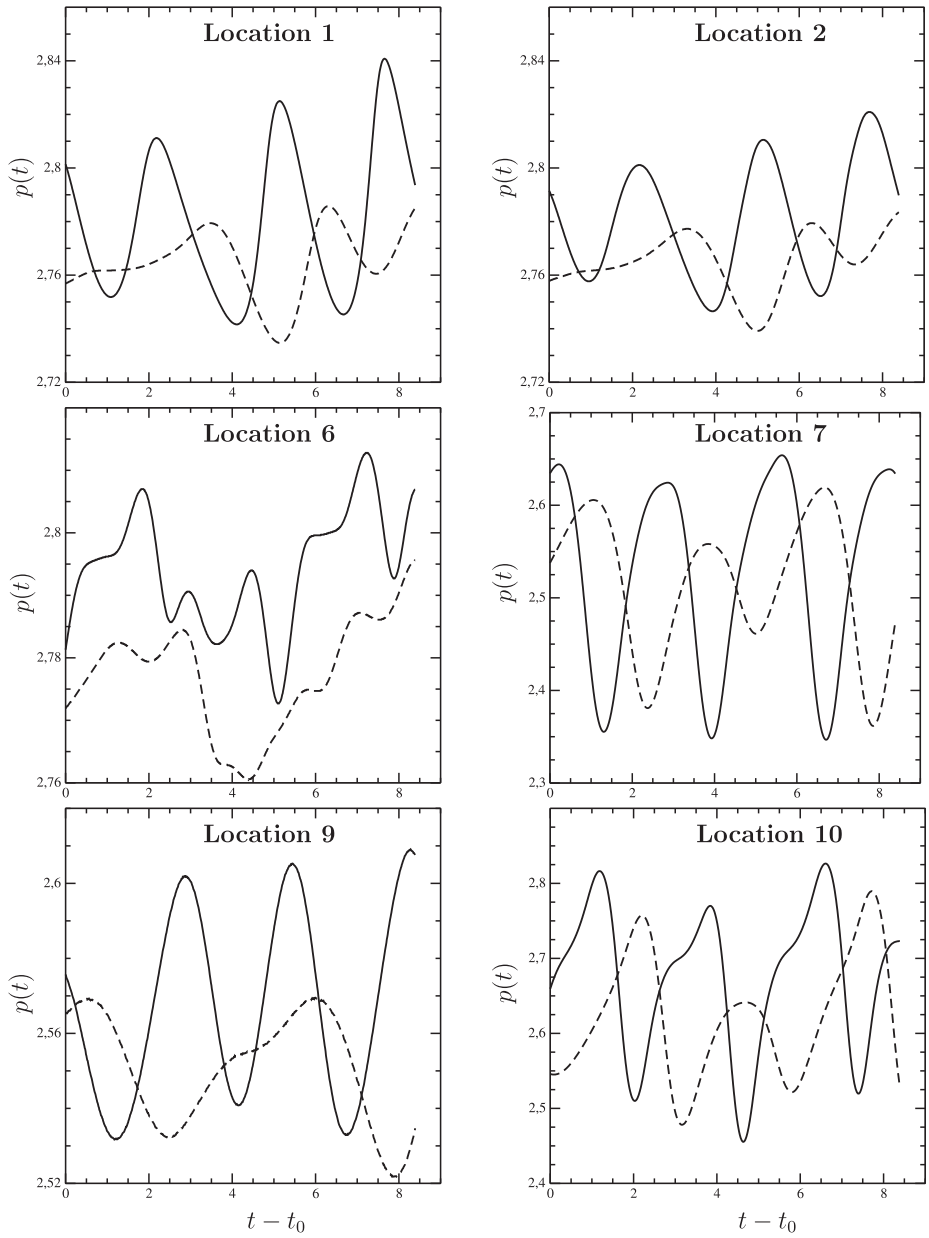

Fig. 14. Comparison of the non-dimensional pressure signals at various locations of the cavity between the uncontrolled flow (solid line) and optimized controlled flow (dashed line). t_0 is an arbitrary time instant.

is found within the frequency range of the temporal excitation γ_e (see Fig. 9) and in the range of the expected physical flow frequency. Indeed, the spectrum shows that the optimal forcing acts at the natural frequency of the unactuated flow *i.e.* at $f = 0.34$. It is as if the optimal control approach provides the physical anti-phase control solution. Fig. 12 represents the evolution of the temporal coefficients obtained by integrating (7) with the optimized control function γ_{opt}. As expected, a significant reduction in the amplitude of the temporal modes is found. We also observe that the mean values of the time coefficients remain very close to zero. The effect of the control law is to decrease the unsteadiness level of the state solution and probably the noise emission of the real flow.

The phase portraits of the optimized controlled flow are shown in Fig. 11 for the temporal coefficients a_2–a_5 plotted against a_1. Clearly, the dynamics is drawn to a specified area of the phase space. This attractor corresponds to an equilibrium state of the high-fidelity forced cavity flow. For this reason, the optimized control γ_{opt} can be considered effective over an infinite (large) time horizon. The main effect of the actuation is to damp the first two POD modes which are the most representative of the uncontrolled flow.

Unlike the Trust-region POD approach [3,13] where there is a mathematical guarantee that the solution determined with the POD-based optimal control approach converge to the one obtained by the high-fidelity model, there is no such guarantee with the simpler framework developed in this paper. The optimal control law γ_{opt} is then introduced into the numerical simulation to check not only the reduction of unsteadiness in the actuated flow but mainly the reduction of noise levels in the cavity. From the careful analysis of the high-fidelity controlled simulations and from additional work not discussed here [1], an explanation of the actuation effect is proposed. The unsteady actuation is located very close to the highest sensitivity zone of the flow, the upstream cavity corner. By a complex but quasi-linear receptivity mechanism, the Kelvin–

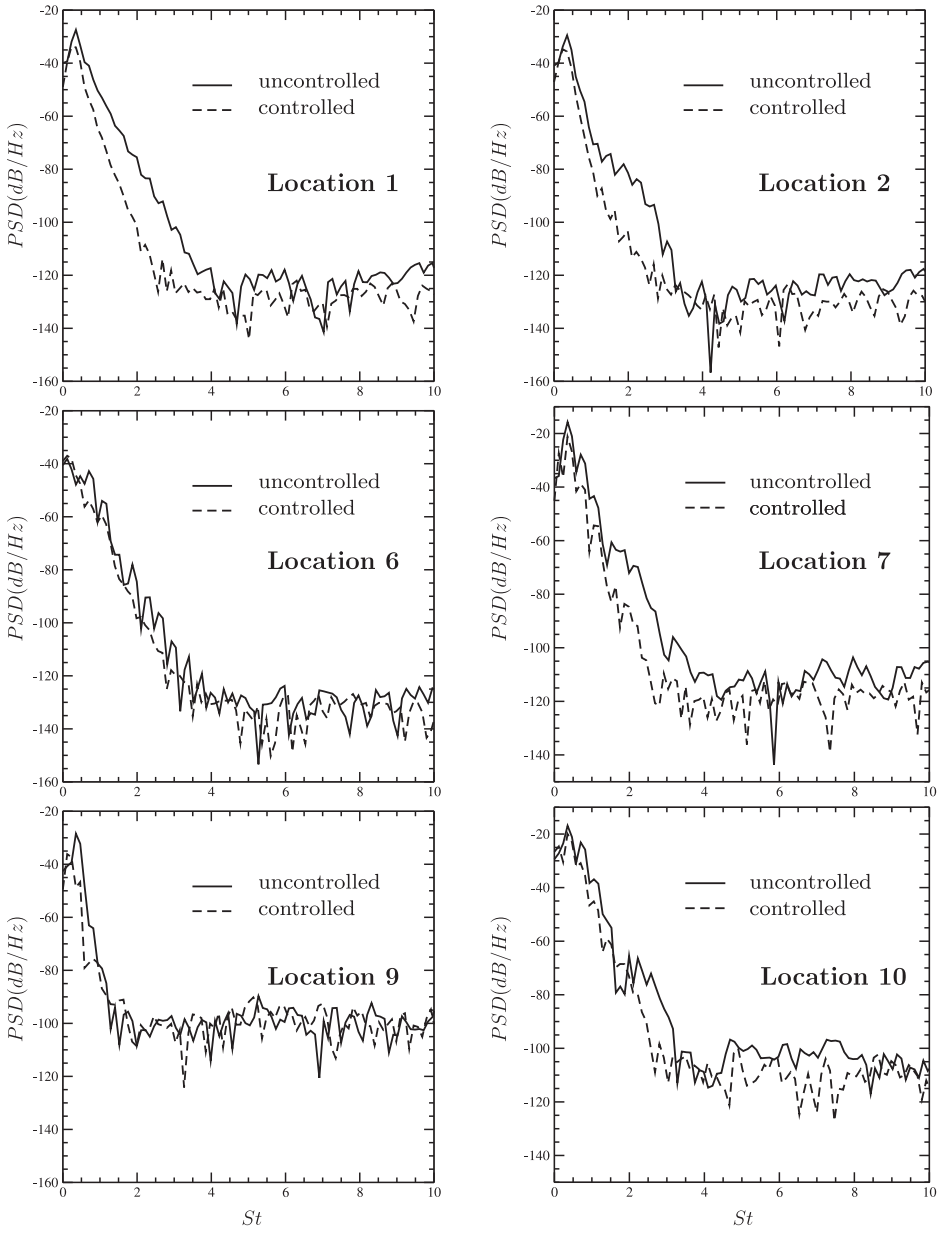

Fig. 15. Comparison of Power Spectral Density (PSD) at various locations of the cavity between the uncontrolled flow (solid line) and optimized controlled flow (dashed line). The PSD is estimated with the classical Welch's method. The time series is multiplied with an Hanning function to reduce the bias in the periodogram.

Helmholtz (KH) instabilities are modified, resulting in a change of the impingement on the downstream corner. It can be observed that the KH structures are slightly deviated downward, reducing the number of direct impact on the downstream corner. Finally, all the feedback loop mechanism inside the cavity is modified, leading to a reduction of the unsteadiness of the pressure fluctuations. At the end, it results in noise reduction and a change of the spatial distribution of the local minimum and maximum of pressure fluctuations of the whole flow. To emphasize this, pressure signals have been sampled at various locations in the shear layer and above the cavity (see Fig. 13) to estimate the efficiency of the optimized control law in terms of noise emission. Fig. 14 represents a comparison of the non-dimensional pressure signals for the uncontrolled flow and optimized controlled flow. At all the sensor locations, the amplitude of the pressure signals is substantially reduced suggesting that the minimization of the state variables unsteadiness also lead to the reduction of the pressure unsteadiness. The complex time evolution of the fluctuations are the results of the significant variations of the local frequency content. The spectra reported in Fig. 15 show an overall decrease in sound pressure level in the frequency range of interest for this configuration, and specifically around the dominant frequency of γ_{opt}. An important reduction larger than 10 dB can be observed in the far field, for instance for the sensors 1 and 2, and on a large frequency bandwidth up to 4. For higher frequencies, the actuation effect is insignificant but the noise level is already negligible. The sixth sensor is located in the zone of highest directivity (see Fig. 5). The effect of actuation on this particular spectrum is less pronounced than for the other sensors. This is further emphasized in Fig. 16.

The OverAll Sound Pressure Level (OASPL) for the uncontrolled and optimized controlled flow are shown in Fig. 16(a) and (b), respectively. The actuation effect can be observed in the whole domain, and more especially at the downstream cavity corner and in the zone of highest directivity. The variations of OASPL linked to the introduction of the optimized actuation in the high-fidelity simulation are shown on Fig. 16(c). These variations are estimated

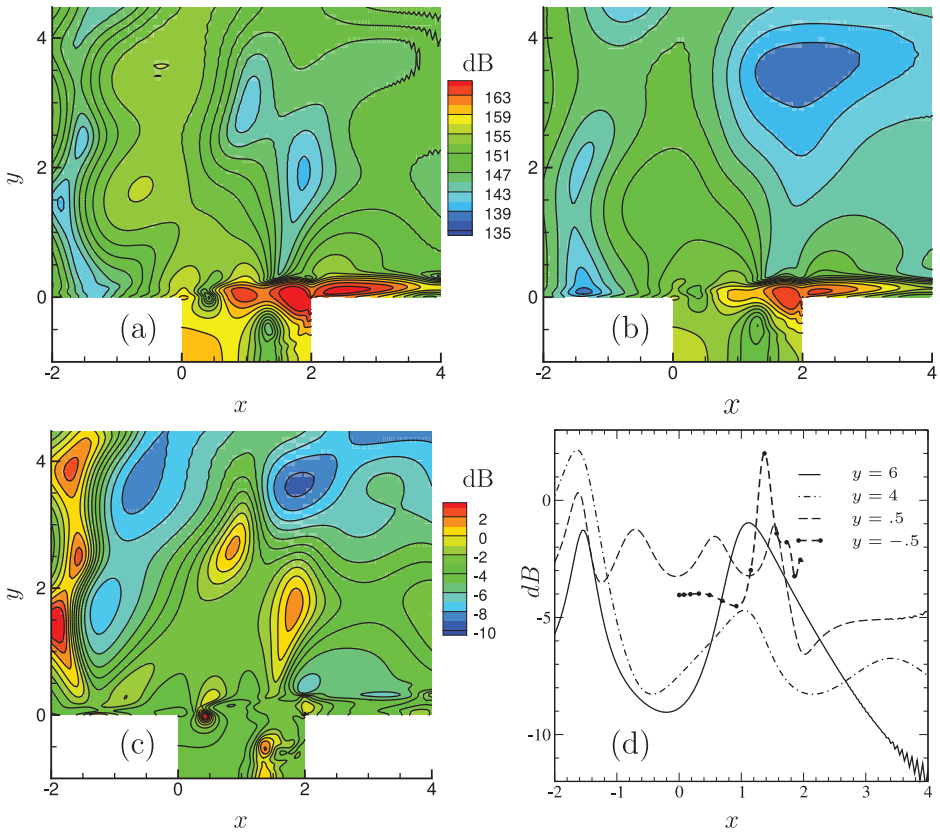

Fig. 16. Contours of the Overall SPL (OASPL) levels in the most relevant part of the computational domain. (a): uncontrolled flow and (b): optimized controlled flow. The same range of contours is used for (a) and (b). (c): Difference of OASPL i.e. Δ(OASPL), see the definition in the text. (d): Streamwise variations of Δ(OASPL) at four vertical positions y.

Table 1
Values of Δ(OASPL) in the two computational blocks. The cavity block is defined by $y<0$ and the upper block by $0\le y\le 6$ and $-2\le x\le 6$. $\langle\Delta(\text{OASPL})\rangle_S$: spatially weighted average of Δ(OASPL); $\Delta(\text{OASPL})_{\min}$ and $\Delta(\text{OASPL})_{\max}$: minimum and maximum values of Δ(OASPL), respectively.

Block	$\langle\Delta(\text{OASPL})\rangle_S$	$\Delta(\text{OASPL})_{\min}$	$\Delta(\text{OASPL})_{\max}$
upper	−5.28	−16.4	5.2
cavity	−3.03	−4.7	4.3

as $\Delta(\text{OASPL}) = \text{OASPL}_{\text{opt}} - \text{OASPL}_{\text{unc}}$ where $\text{OASPL}_{\text{opt}}$ and $\text{OASPL}_{\text{unc}}$ stand for optimized and uncontrolled flow, respectively. Locally, near $x=-2$, and in some isolated areas above the cavity, an increase of noise level up to 3 dB is observed. However, the dominant trend is the reduction of noise level. The highest reduction is obtained in a slightly inclined band upstream the cavity, in the region downstream the cavity and in the far field for $y>4$ and $x>3$.

To quantify in a more global way the noise variations induced by the control, we define for the two computational blocks (cavity and upper block) $\langle\Delta(\text{OASPL})\rangle_S$, the weighted spatial average of Δ(OASPL). The results are reported in Table 1 with the minimum and maximum values of Δ(OASPL). The maximum increase of noise level in the cavity is quite large (4.3 dB), compared to the value of the weighted spatial average in this block that is equal to −3.03 dB. However, this maximum is localized in a very small area, just in the middle of the shear layer. As stated before, the actuation modifies the shear layer receptivity and therefore some strong variations of noise level can be expected in this region. The value of the weighted spatial average in the upper block is equal to −5.28 dB. This value is combined with a large amplitude of variation of Δ(OASPL), about 22 dB from minimum to maximum. Since the noise reduction increases in the far field, extending the upper domain used for the averaging will lead to a decrease of the weighted spatial average value.

To further analyze the variations of OASPL, Δ(OASPL) are plotted along the streamwise direction for four values of y, see Fig. 16(d). For $y=-0.5$ (inside the cavity), a local peak at 3 dB is trapped in the cavity, as it is clearly visible in Fig. 16(c). Some oscillations of Δ(OASPL) are observed in the upper block, just above the cavity ($y=0.5$). These oscillations are due to the shear layer instability which plays a crucial role in the flow dynamic and in the flow aeroacoustic as shown in the dilatation plots of the POD modes (Fig. 5). At larger vertical positions ($y=4$ and $y=6$), the influence of the KH instability disappears. Two large peaks emerge upstream the cavity and just at the vertical of the cavity center. Two large minimum are also present at the level of the cavity upstream corner and just above the cavity downstream corner. At the far field ($y=6$), the noise level decrease is between 1 dB and 9 dB. Far downstream the cavity, the noise level continues to decrease but with lesser meaning, considering that the noise levels in the flow is naturally low.

5. Conclusion

In this paper, we minimized the noise emitted from a low-Reynolds compressible two-dimensional flow past a cavity with a reduced-order optimal control approach based on POD modes. For that, a direct numerical simulation of the compressible Navier–Stokes equations was performed to obtain unactuated flow solutions at different time instants. Based on these snapshots, a Proper Orthogonal Decomposition was applied to extract dominant modes

in terms of an inner product based on the enthalpy norm. A reduced-order model of the unactuated dynamics was then derived by a Galerkin projection of the isentropic Navier–Stokes equations onto the first POD modes. To improve the long term accuracy of the reduced-order model, an identification procedure was used to determine the coefficients of the model. In a second step, this unactuated model was augmented with a particular control input separation method, leading to the determination of a spatial actuation mode. The robustness of the model to the variation of the control parameters was further strengthened by using an ensemble of actuated snapshots corresponding to chirp-forced transients. This actuated reduced-order model was employed in an adjoint-based optimal control approach to minimize the total enthalpy unsteadiness. Finally, the optimized control law was introduced into the high-fidelity model to prove the optimality in terms of noise reduction. As a result, a maximum noise reduction of 4.7 dB has been reached in the cavity and more than 16 dB at the far-field downstream the cavity. Locally in the near field, some pressure waves are trapped and increased the noise level without large propagation. An attempt to explain the effect of the actuation on the flow physics has been proposed. We claim that the actuation disturbs the receptivity mechanism of the shear layer in such a way that the KH structures no longer impact directly the downstream cavity corner, reducing the intensity of the well-known feedback loop mechanism.

Given the low computational costs needed for solving an optimization problem with a POD ROM, we can conclude that using reduced-order models for solving a constrained optimization problem is a key strategy. However, one drawback of that approach is the lack of mathematical proof that the solution of the optimization problem with the approximation model will correspond to the solution of the optimization problem with the original high-fidelity model.

Many directions of improvement can be considered as perspectives. The first idea is to increase the Reynolds number and to change the cavity configuration to assess the interest of the method for more complex flow configurations. One aim could be to extend the methodology to investigate flow control in some three-dimensional turbulent flows. For that, a number of challenges need to be addressed. First, accurate 3D simulations of turbulent flows with actuation effect need to be developed. Second, turbulence scales need to be properly introduced into the POD ROM. Third, an effective control strategy need to be implemented for determining a physically interesting equilibrium state of the controlled flow.

Further simpler improvements can be carried out. The inner product in the POD analysis and the governing equations employed in the Galerkin projection can be modified, see for instance Zhang et al. [37] where a POD ROM was constructed involving primitive variables of the fully compressible Navier–Stokes equations. Concerning the chirp actuation law, used for extracting the actuation mode and defining the generalized POD modes, its influence should be evaluated as well. The last obvious direction is to modify the definition of the objective functional by using another noise-related function based on the pressure evolution in a certain region of the far-field [28, for instance]. Another promising extension of the current work is to correlate the near-field hydrodynamics to the far-field acoustics to obtain a suitable plant model as demonstrated in Schlegel et al. [34]. Another possible extension is to apply the Trust-Region POD framework developed in Bergmann and Cordier [3] for which there is a mathematical assurance that the optimal solution based on the POD ROM corresponds to a local optimizer for the high-fidelity model. Finally, we can envision to apply a model-free control strategy based on *Genetic Programming* [12] to determine in an unsupervised manner a closed-loop control law leading to the maximum noise reduction.

Acknowledgment

L.C. acknowledges the funding of the ONERA/Carnot project INTACOO (INnovaTive ACtuators and mOdels for flow cOntrol). The authors appreciate valuable stimulating discussions with Bernd R. Noack on model-based control. A part of the work has been funded under the ANR (grant no. ANR-08-BLAN-0115-02) (National French Research Agency) project CORMORED and the Marie Curie Project AeroTraNet. KKN and SS would like to appreciate the support of Mathur J. S. and Ramesh V. of CTFD division NAL for their encouragement during the course of this work. The authors would like to acknowledge the first reviewer for his/her valuable comments that greatly contributed to improve the content of this paper.

Appendix A. A non convex optimization approach to handle the acoustic terms

To minimise the acoustic noise one defines a functional based on the dilatation operator defined by

$$\begin{aligned} \mathcal{D} \quad &: \quad H^2(\Omega) \longrightarrow \mathbb{R} \\ (u, v, c) \longrightarrow &\int_\Omega (u_x + v_y)^2 \, d\Omega \end{aligned} \tag{14}$$

The flow field expansion for the actuated case can be written as

$$q = \overline{q} + \gamma(t)\psi + \sum_{i=1}^{n} a_i(t)\phi_i \tag{15}$$

On applying the operator $\mathcal{D}$ we obtain

$$\begin{aligned} \mathcal{D}(q) &= \mathcal{D}(\overline{q}) + \gamma(t)\mathcal{D}(\psi) + \sum_{i=1}^{n} a_i(t)\mathcal{D}(\phi_i) \\ &= P + \gamma(t)M + \sum_{i=1}^{n} a_i(t)N_i \end{aligned} \tag{16}$$

For the optimisation problem we propose to minimise the functional given by

$$\begin{aligned} \tilde{\mathcal{J}}(a) &= \int_0^T \mathcal{J}(a)dt \quad \text{where} \\ \mathcal{J}(a) &= \sum_{i=1}^{n} a_i(t)N_i \end{aligned} \tag{17}$$

The above definition of the functional gives the time average of the dilatation over the period of optimization. Also note that the above definition of our functional is not quadratic unlike the definition we have used before and hence the process does not guarantee a minimiser. The constrained optimization can be now written as

$$\begin{cases} \min_{(\gamma,a)} \tilde{\mathcal{J}}(a,\gamma) \\ \qquad\qquad \text{s.t.} \\ \mathcal{N}(a,\gamma) = 0 \end{cases}$$

The Lagrangian for the above problem can be defined as can be defined by introducing the adjoint variable ξ

$$\begin{aligned} \mathcal{L}(a,\gamma,\xi) &= \tilde{\mathcal{J}}(a,\gamma) - \langle \xi, \mathcal{N}(a,\gamma) \rangle \\ &= \tilde{\mathcal{J}}(a,\gamma) - \sum_{i=1}^{n} \int_0^T \xi_i(t)\mathcal{N}_i(a,\gamma)dt \end{aligned} \tag{18}$$

minimisation of the above functional with respect to the state variable a gives the adjoint equations

$$\frac{d\xi_i(t)}{dt} = -\sum_{i=1}^{n} \left(L_{ij} + \gamma(t)h_{2ij} + \sum_{i=1}^{n} \left(Q_{jik} + Q_{jki}\right)a_k(t) \right) \xi_j(t) - N_i \tag{19}$$

with the terminal condition given by

$$\xi_i(T) = 0$$

The optimality system obtained by finding the stationary value with respect to the control parameter γ is given as

$$\Delta_\gamma \mathcal{L} = \int_0^T \sum_{i=1}^{n} P_i \nabla\gamma \, \mathrm{dt} \tag{20}$$

where

$$P_i = \sum_{i=1}^{n} \left(h_{1i} + \sum_{j=1}^{n} h_{2ij} a_j + 2h_{3i}\gamma(t) \right) \xi_i$$

References

[1] Airiau C, Cordier L. Flow control of a two-dimensional compressible cavity flow using direct output feedback law. Contrôle des décollements. Separated flow control and aerodynamic performance improvements. Cépaduès, editor; 2013. ISBN 978-2-3649-3085-8.

[2] Benner P, Gugercin S, Willcox K. A survey of projection-based model reduction methods for parametric dynamical systems. SIAM Rev 2015;57(4):483–531. doi:10.1137/130932715.

[3] Bergmann M, Cordier L. Optimal control of the cylinder wake in the laminar regime by trust-region methods and POD reduced-order models. J Comp Phys 2008;227:7813–40.

[4] Bergmann M, Cordier L, Brancher J-P. Optimal rotary control of the cylinder wake using POD reduced-order model. Phys Fluids 2005;17(9). 097101:1–21.

[5] Bres GA, Colonius T. Three-dimensional instabilities in compressible flow over open cavities. J Fluid Mech 2008;599:309–39.

[6] Brunton SL, Noack BR. Closed-loop turbulence control: progress and challenges. App Mech Rev 2015;67:5.

[7] Cordier L. Flow control and constrained optimization problems. In: Noack BR, Morzyński M, Tadmor G, editors. Reduced-order modelling for flow control. CISM International Centre for Mechanical Sciences, 528. Springer-Verlag; 2011. p. 1–76. ISBN 978-3-7091-0757-7.

[8] Cordier L, Abou El Majd B, Favier J. Calibration of POD reduced-order models using Tikhonov regularization. Int J Numer Meth Fluids 2009;63(2):269–96.

[9] Cordier L, Bergmann M. Proper orthogonal decomposition: an overview. In: Lecture series 2002-04, 2003-03 and 2008-01 on post-processing of experimental and numerical data. Von Kármán Institute for Fluid Dynamics; 2008. p. 1–46. ISBN 978-2-930389-80-X.

[10] Cordier L, Bergmann M. Two typical applications of POD: coherent structures eduction and reduced order modelling. In: Lecture series 2002-04, 2003-03 and 2008-01 on post-processing of experimental and numerical data. Von Kármán Institute for Fluid Dynamics; 2008. p. 1–60. ISBN 978-2-930389-80-X.

[11] Couplet M, Basdevant C, Sagaut P. Calibrated reduced-order POD-Galerkin system for fluid flow modelling. J Comp Phys 2005;207:192–220.

[12] Duriez T, Brunton S, Noack BR. Machine learning control — taming nonlinear dynamics and turbulence. No. 116 in fluid mechanics and its applications. Springer-Verlag; 2016.

[13] Fahl M. Trust-region methods for flow control based on reduced-order modeling. Trier University; 2000. Ph.d. thesis.

[14] Gloerfelt X. Compressible proper orthogonal decomposition/Galerkin reduced-order model of self sustained oscillations in a cavity. Phys Fluids 2008;20:115105.

[15] Gloerfelt X, Bailly C, Juvé D. Direct computation of the noise radiated by a subsonic cavity flow and application of integral methods. J Sound Vib 2003;266(1):119–46.

[16] Gottlieb D, Turkel E. Dissipative two-four method for time dependent problem. Tech. Rep.. No. 75-22: Courant Institute of Mathematical Sciences, New-York University; 1975.

[17] Gunzburger MD. Introduction into mathematical aspects of flow control and optimization. Lecture series 1997-05 on inverse design and optimization methods. Von Karman Institute for Fluid Dynamics; 1997.

[18] Gunzburger MD. Lagrange multiplier techniques. Lecture series 1997-05 on inverse design and optimzation methods. Von Karman Institute for Fluid Dynamics; 1997.

[19] Gunzburger MD. Perspectives in flow control and optimization. SIAM; 2003.

[20] Holmes P, Lumley JL, Berkooz G. Turbulence, coherent structures, dynamical systems and symmetry. Cambridge University Press, Cambridge, U.K.; 1996.

[21] Huerre P, Rossi M. Ch. hydrodynamics and nonlinear instabilities. In: Hydrodynamic instabilities in open flow. Cambridge University Press; 1998. p. 81–294.

[22] Kalb VL, Deane AE. An intrinsic stabilization scheme for proper orthogonal decomposition based low-dimensional models. Phys Fluids 2007;19:054106.

[23] Kasnakoglu C. Reduced-order modeling, nonlinear analysis and control methods for flow control problems. Ohio State University; 2007. Ph.d. thesis.

[24] Moret-Gabarro L. Aeroacoustic investigation and adjoint analysis of subsonic cavity flows. Institut National Polytechnique de Toulouse; 2009. Ph.D. thesis.

[25] Nagarajan KK. Analysis and control of self-sustained instabilities in a cavity using reduced-order modelling. Institut National Polytechnique de Toulouse; 2010. Ph.D. thesis.

[26] Nagarajan KK, Cordier L, Airiau C. Development and application of a reduced-order model for the control of self-sustained instabilities in a cavity flow. Commun Comput Phys 2013;14(1):186–218.

[27] Noack BR, Morzynski M, Tadmor G, editors. Reduced-order modelling for flow control. CISM courses and lectures 528. Springer-Verlag; 2010.

[28] Otero J.J., Sharma A.S., Sandberg R.D.. Adjoint-based optimal flow control for compressible DNS. arXiv:1603058872016;.

[29] Perret L, Collin E, Delville J. Polynomial identification of POD based low-order dynamical system. J Turbul 2006;7:1–15.

[30] Rowley CW, Colonius T, Basu AJ. On self-sustained oscillations in two-dimensional compressible flow over rectangular cavities. J Fluid Mech 2002;455:315–46.

[31] Rowley CW, Colonius T, Murray RM. Model reduction for compressible flows using POD and Galerkin projection. Physica D Nonlinear Phenom 2004;189(1–2):115–29.

[32] Rowley CW, Williams DR. Dynamics and control of high-Reynolds number flow over cavities. Ann Rev Fluid Mech 2006;38:251–76.

[33] Samimy M, Debiasi M, Caraballo E, Serrani A, Yuan X, Little J, et al. Feedback control of subsonic cavity flows using reduced-order models. J Fluid Mech 2007;579:315–46.

[34] Schlegel M, Noack BR, Jordan P, Gröschel E, Schröder W, Wei M, et al. On least-order representations for aerodynamics and aeroacoustics. J Fluid Mech 2012;697:387–98.

[35] Sipp D, Schmid PJ. Linear closed-loop control of fluid instabilities and noise-Induced perturbations: A Review of approaches and tools. ASME Appl Mech Rev 2016;68(2):020801–020801–26. doi:10.1115/1.4033345.

[36] Sirisup S, Karniadakis GE. A spectral viscosity method for correcting the long-term behavior of POD model. J Comp Phys 2004;194:92–116.

[37] Zhang C, Wan Z, Sun D. Model reduction for supersonic cavity flow using proper orthogonal decomposition (POD) and Galerkin projection. Appl Math Mech 2017;38(5):723–36.